THE UNIVERSITY of EDINBURGH

Edinburgh Research Explorer

The phonon spectrum of phase-I ammonia: Reassignment of lattice mode symmetries from combined molecular and lattice dynamics calculations

OPEN ACCESS

The Phonon Spectrum of Phase-I Ammonia: Reassignment of Lattice Mode Symmetries from Combined Molecular and Lattice Dynamics Calculations**

Anthony M. Reilly,[1] Derek S. Middlemiss,[2] M. Murshed Siddick,[1] Derek A. Wann,[1] Graeme J. Ackland,[3] Chick C. Wilson,[2] David W. H. Rankin[1] and Carole A. Morrison[1,*]

[1]EaStCHEM, School of Chemistry, Joseph Black Building, University of Edinburgh, West Mains Road, Edinburgh, EH9 3JJ, UK.

[2]Department of Chemistry, University of Glasgow, University Avenue, Glasgow, G12 8QQ, UK.

[3]School of Physics, University of Edinburgh, Mayfield Road, Edinburgh, EH9 3JZ, UK.

[*]Corresponding author; e-mail: c.morrison@ed.ac.uk

Supporting information:
XYZ format trajectory files of the eigenvectors for each of the NH3 and ND3 lattice modes. Graphs of temperature and energy for the MD runs. This material is available free of charge via the Internet at http://pubs.acs.org

Abstract:

The zone-center phonon spectra of phase-I ammonia and deuterated ammonia have been obtained from plane-wave DFT molecular dynamics and localized basis set harmonic lattice dynamics simulations. These data have proved to be excellent for benchmarking the two approaches. Significant changes to the assignments of the experimental low-frequency lattice modes are proposed on the basis of the calculated data. The magnitude of the splitting of the longitudinal and transverse optical modes has been determined and is shown to be significant in some cases. The high-frequency internal mode region of the spectrum has also been obtained and is shown to be in excellent agreement with the results of previous studies. The symmetry coordinates and Davydov splittings of the internal modes are fully analyzed.

1. Introduction

The phonon spectrum of a molecular solid typically comprises a region dominated by the high frequency internal vibrations of molecules (*i.e.* bond stretches, angle bends *etc.*) along with the low frequency external vibrations of the system (*i.e.* motions of the molecules relative to each other). Phonon spectra often prove quite difficult to interpret and assign correctly, for whereas an isolated *N*-atom molecule possesses 3*N*-6 normal modes of vibration, the unit cell of a molecular crystal typically contains multiple molecules, the vibrations of each of which combine with the external motions to form the larger set of lattice modes. The system upon which this paper focuses, phase I ammonia, provides an excellent example of the difficulties encountered. The NH_3 molecules condense into a cubic structure ($P2_13$ space group) with a lattice constant of 5.1305(8) Å at 160 K.[1] The unit cell contains four molecules, and the Γ-point phonon spectrum comprises 48 modes,[2] as compared with the six modes obtained for the isolated molecule. Taking account of the degeneracy of the modes leads us to expect 19 distinct peaks in the experimental spectra. Whilst a wealth of literature[2-7] spanning nearly 60 years has been devoted to the study of the vibrational properties of this material, no clear and full assignment has been forthcoming.

The confusion over the ammonia phonon spectrum arises mainly in the lattice-mode region of the spectrum. Brinbrek and Anderson[3] provided the original assignments for the symmetries of the lattice modes based upon infra-red (IR) and Raman spectroscopy. Righini *et al.*[4] performed empirical model calculations with the aim of reproducing the experimental modes as closely as possible, in order to explore the dynamics of the system further. This latter study resulted in significant variations in the symmetry assignments from those proposed by Brinbrek and Anderson. The experimental studies also include an application of coherent inelastic neutron scattering (C-INS) to deuteroammonia by Powell *et*

al.,[5] which also suggested changes to the assignments made by Brinbrek and Anderson but did not agree completely with the theoretical assignments of Righini *et al*. Our group has recently conducted a study of the low-frequency modes in ammonia based on constrained molecular dynamics (MD) simulations.[2] A method of extracting the eigenvectors of a particular mode from the MD trajectory was applied, permitting us to examine selected atomic displacement patterns and to reassign tentatively some of the previously accepted mode symmetries.

The disagreements in the experimental assignments of the phonon spectrum are not unexpected, for each of the techniques applied suffers from its own inherent set of difficulties. The observability of certain modes in IR and Raman spectroscopy is often limited by the effects of the selection rules and by the weak coupling of certain motions to the probe radiation. The existence of combination and overtone bands can lead to considerable confusion, as can the erroneous assignment of split longitudinal- (LO) and transverse optical (TO) modes in polar compounds. This latter effect arises from the lifting of the degeneracy of some of the modes at the Γ-point due to long-range electrostatic interactions, leading to the appearance of more peaks in the spectrum than would be expected from the group theory analysis alone. It is also possible that the introduction into the lattice of defects such as vacancies or interstitials may produce localized modes that appear in measured spectra. Given these potential complications, it is now common practice to augment the experimental observations with a theoretical determination of the spectra. While isolated molecule calculations can be of use in this regard, solid-state approaches are to be preferred, the most commonly applied of which are the molecular– and lattice dynamics methods.

Molecular dynamics (MD) simulations furnish a continuous trajectory for a system by integration of the atomic equations of motion at a series of discrete time steps. MD simulations can provide an extensive range of physical properties for a material, including thermodynamic functions, diffusion constants and elastic properties etc. In the current application we calculate the velocity autocorrelation function[8] (VAF), which may be Fourier transformed to obtain the normal modes of motion of a material. MD simulations based upon the forces obtained from density functional theory (DFT) have recently become much more commonplace. Alongside the natural incorporation of anharmonic effects in the MD

approach in general, such DFT-MD simulations offer the further advantage of including the instantaneous changes in the electronic structure and bonding of a material due to atomic motion. The inclusion of both of these effects has been shown to be important if close agreement with experimental data is sought. However, DFT-MD calculations are generally computationally intensive and may as a consequence be capable of providing only short trajectories, whereas obtaining adequate spectral resolution of low frequency modes usually requires long sampling times. This problem can be partially overcome by convolution of the VAF with a windowing function[9] prior to Fourier transformation, in effect limiting the error due to the finite extent of the dataset. Non-ergodicity of the system can also be a problem in short simulations, but this can be addressed by use of thermostats that effectively enforce the proper equipartitioning of the energy. We note also that the extraction of frequency-specific eigenvectors from MD simulations is an uncommon practice,[10-12] and that the assignment of the symmetry of the motions, which must currently be done by hand, might become a difficult task in large, complex systems.

Lattice dynamics calculations approach the problem of obtaining the normal modes from a different perspective altogether, and seek to solve the strictly harmonic atomic equations of motion by direct diagonalization of the dynamical matrix.[13] Density functional perturbation theory or frozen-phonon methods can both be generally applied to determine the Γ-point modes and also the full phonon dispersion relations throughout the reciprocal space zone.[14] The method offers a number of advantages over MD simulations, amongst the most useful of which is the implicit inclusion of crystal symmetry and the provision of correctly symmetrized eigenvectors for each mode that require no assignment. Further, no issues relating to the sampling of low-frequency modes or ergodicity arise, and the calculations are typically much less intensive than comparable MD simulations on the same system. The technique may be efficiently implemented alongside any total energy calculation scheme that provides numerically accurate gradients, freeing us to apply any Hamiltonian we choose to the task of calculating the phonon spectra. In the current study we make use of this fact, and compare the modes obtained from various pure and hybrid DFT functionals. Lattice dynamics calculations can also be readily extended to

include the LO-TO splitting effect, through the addition to the Γ-point dynamical matrix of a correction term that depends in a non-trivial manner on the lattice polarity and the high-frequency dielectric constant tensor, ε^{∞}. MD simulations can also capture at least a part of the splitting, but the long-range nature of the electrostatic interactions involved mandates the use of large supercells. Such large supercells are also required for MD simulations to probe non-Γ-point modes. Alongside the strengths of the method, however, we emphasize again that lattice dynamics calculations are rooted within a strictly harmonic approximation, and that this may be a poor representation of the true potential-energy surface underlying some motions. Any deficiencies due to this effect are most likely to manifest themselves in the nitrogen-proton stretching modes in the current study. We note also that the lattice modes are also particularly sensitive to inaccuracies in the calculation of the dynamical matrix.

The current work focuses upon the phase I ammonia structure, the compact cell of which makes it well suited to simulations, and for which a large number of experimental studies of the vibrational properties exist. We seek in particular to estimate the size of the LO-TO splitting, for it has often been invoked in previous experimental assignments of the modes.[2,3] The isotopic frequency shifts have also previously assisted the interpretation of the experimental spectra[5] and, in particular, provide a means by which the low frequency modes can be classified into librational and translational types (as discussed in Section 3.3). We obtain comparable theoretical values for both methods from simulations of the fully protonated (NH_3) and deuterated (ND_3) lattices. Section 2 gives details of the computational techniques applied, while the equilibrium geometries obtained from the various methods are presented in Section 3.1. The results for the low-frequency region of the protonated spectrum are presented in Section 3.2 along with a mode-by-mode assignment. The corresponding region of the deuterated lattice spectrum is discussed in Section 3.3. Finally, we discuss the internal mode region of both isotopic forms.

2. Theoretical Methods

2.1. Molecular Dynamics Calculations. The geometry of the ammonia unit cell was optimized from the initial experimental structure[15] within the CASTEP plane-wave pseudopotential DFT code.[16] The PW91 GGA-type exchange–correlation functional was used, together with a plane-wave cut-off energy of 400 eV. Core–valence interactions were represented by standard ultrasoft pseudopotentials, and the reciprocal space zone was sampled upon a 2×2×2 Monkhorst-Pack grid. A mesh of this density suffices to converge the atomic forces and maximum stress tensor component in a trial distorted geometry to better than 0.001 in 0.172 eV Å^{-1}, and 0.02 in 0.93 GPa respectively. Variable volume geometry optimizations were pursued until the energy change per atom, maximum atomic force and maximum stress component fell below tolerances of 5×10^{-7} eV, 1 meV Å^{-1} and 0.02 GPa respectively. The subsequent NVE-ensemble molecular dynamics simulation was performed within the NH_3 unit cell and proceeded from this initial geometry. The initial temperature of 155 K quickly equilibrated to a steady 77 K. The position and velocity of, and force acting upon, each atom in the cell were obtained at intervals of 0.5 fs, where this timestep was chosen to ensure adequate sampling of the high-frequency N–H stretching motions. Data were collected for 30 ps in total. A comparable MD simulation for ND_3 was also performed with the same parameters, save that a longer time step of 0.8 fs was used, reflecting the fact that a lower stretching frequency was anticipated for the N–D bond. This run also maintained a steady temperature of 77 K after equilibration, and data were again collected for 30 ps.

The eigenvalues of the phonons were extracted from the NH_3 and ND_3 trajectories via the standard VAF method, and the associated eigenvectors were obtained as described in our previous work.[2] The Fourier transform of the VAF is sensitive to both the finite length of the dataset and to the amplitudes of the modes being extracted, but we counter these problems by application of various Blackman windowing functions[9] with widths of 10, 7.5 and 5 ps. Wider windows lead to greater errors in the small amplitude modes (*i.e.* the internal vibrations) but allow better resolution of the low-frequency modes.

2.2. Lattice Dynamics Calculations. The geometry of phase I ammonia at equilibrium was determined within a range of Hamiltonians and localised basis sets by optimizations using the

6

CRYSTAL06 code.[17] Optimizations continued until the changes in total energy fell below 2×10^{-7} eV, and the root-mean-squared (RMS) gradients and displacements were below 2.6 meV Å^{-1} and 2.5×10^{-4} Å, respectively. The tolerances for individual components of the gradients and displacements were set at 1.5 times the respective RMS thresholds. SCF convergence tolerances were set at 3×10^{-8} eV per cell, while reciprocal space was sampled with an 8×8×8 Monkhorst-Pack grid, the inexpensive nature of the LD calculations permitting a much more dense mesh to be applied than was the case in the MD simulations. The convergence of forces and stresses with respect to the sampling mesh is therefore superior to that of the MD simulations, but we note that the accuracy of the latter was already more than sufficient. The optimized geometries being obtained, the normal modes of the lattice were determined within these cells by a series of finite displacement calculations, in which a subset of the atoms in the cell were translated by 0.003 Å along each of the Cartesian axes.[18,19] The point group symmetry of the lattice was used to generate the full force-constant matrix from an irreducible set of atomic displacements. In the primitive cell of ammonia, this amounts to the shift of one hydrogen atom along the x, y and z axes and the shift of one nitrogen atom along the x axis. The external mode frequencies obtained from test calculations with tighter optimization and SCF tolerances differed by 1.2 cm^{-1} at most from the values produced by the procedure detailed above. Furthermore, forcing strict adherence to the sum rule through a direct normalization of the dynamical matrix resulted in only negligible variations in the frequencies. The dynamical charges of the lattice were determined by a Wannier localization procedure, and the LO-TO splitting correction term was added to the Γ-point dynamical matrix determined at the B3LYP/6-311G** level of theory. Splittings were calculated for values of ε^{∞} ranging from 1.3 to 2.3, bracketing the experimental value of 1.9 obtained in the liquid phase.[20] A similar determination of the LO-TO splitting was also made for the fully deuterated lattice.

3. Results and Discussion

3.1 Optimized Structures of Phase I NH$_3$

Plane-wave basis set. The optimized structure of ammonia determined in the plane-wave (PW) calculations with the PW91 functional is presented in Table 1. The asymmetric unit of phase I ammonia consists of a single H/D atom and one third of an N atom. Note that the equilibrium structures of NH_3 and ND_3 are identical, as the atomic forces and cell stresses are independent of the nuclear masses. The theoretical cell vector, which is formally obtained at 0 K, is 1% longer than the 160 K experimental value. Similarly, the calculated N–H bond is 2% longer than that measured at 160 K, while the closest H$\cdots$N distance is nearly 3% shorter than the experimental value.

Table 1 The optimized fractional coordinates of phase I ammonia as determined by PW91/PW calculations, together with the optimized lattice constant, a_{opt} (Å), and N–H and H$\cdots$N distances (Å).

H_x	0.3460
H_y	0.2714
H_z	0.0910
N_x	0.1935
a_{opt} / Å	5.1846
r(N–H) / Å	1.0347
r(H$\cdots$N) / Å	2.336

Localized Basis Sets. The optimised structures obtained from our initial calculations using localized basis sets are presented in Table 2. The TZP basis set splits *s* and *p* shells, whereas 6-311G** uses more computationally convenient but less flexible *sp*-shells in which the *s* and *p* primitive functions share a common set of exponents. Despite the use of different basis sets and correlation functionals, the three B3 (*i.e.* 20% Hartree-Fock exchange) hybrid calculations provide similar geometries, with N–H and H$\cdots$N bond lengths that are within 1.0 and 1.4% of the experimental values, respectively. The PW91 bond lengths show larger differences from experiment of 1.8 and 3.1%, respectively. The larger cell vectors obtained from the B3LYP and B3PW91 calculations as compared with the PW91 values are due to small reorientations of the molecules. Finally, we note that the substitution of the less constrained TZP basis for the 6-311G** set lowers the energy of the optimized cell by 0.41 eV, so that the former represents the closest approach to the variational minimum achieved within the current study.

Table 2 The optimized lattice constant, a_{opt} (Å), and N–H and H···N distances (Å) obtained from various electronic Hamiltonians and basis sets, together with the 160 K experimental values.

Method	B3LYP	B3LYP	B3PW91	PW91	Expt[a]
Basis	TZP	6-311G**	6-311G**	TZP	
a_{opt} / Å	5.2562	5.2418	5.2354	5.1408	5.1305
r(N–H) / Å	1.019	1.020	1.020	1.028	1.010
r(H···N) / Å	2.401	2.377	2.365	2.324	2.398

[a] Ref. 1.

3.2. Phase I NH$_3$ Lattice Modes.

MD trajectory. The time-averaged fractional coordinates of the asymmetric unit of NH$_3$ are presented in Table 3. In evaluating these positions the first 4 ps of the trajectory have been discarded to allow for equilibration of the system. Figure 1 shows the lattice-mode region (0–650 cm^{-1}) of the mass-balanced NH$_3$ phonon spectrum determined by Fourier transformation of the convolution of the VAF with the three different Blackman windowing functions. All three spectra show nine distinct peaks, as expected from the group theory analysis of the equilibrium structure.

Table 3 The fractional coordinates of the asymmetric unit in NH$_3$ averaged over the 30 ps PW-DFT MD trajectory.

H$_x$	0.3518
H$_y$	0.2698
H$_z$	0.0965

N_x	0.1972
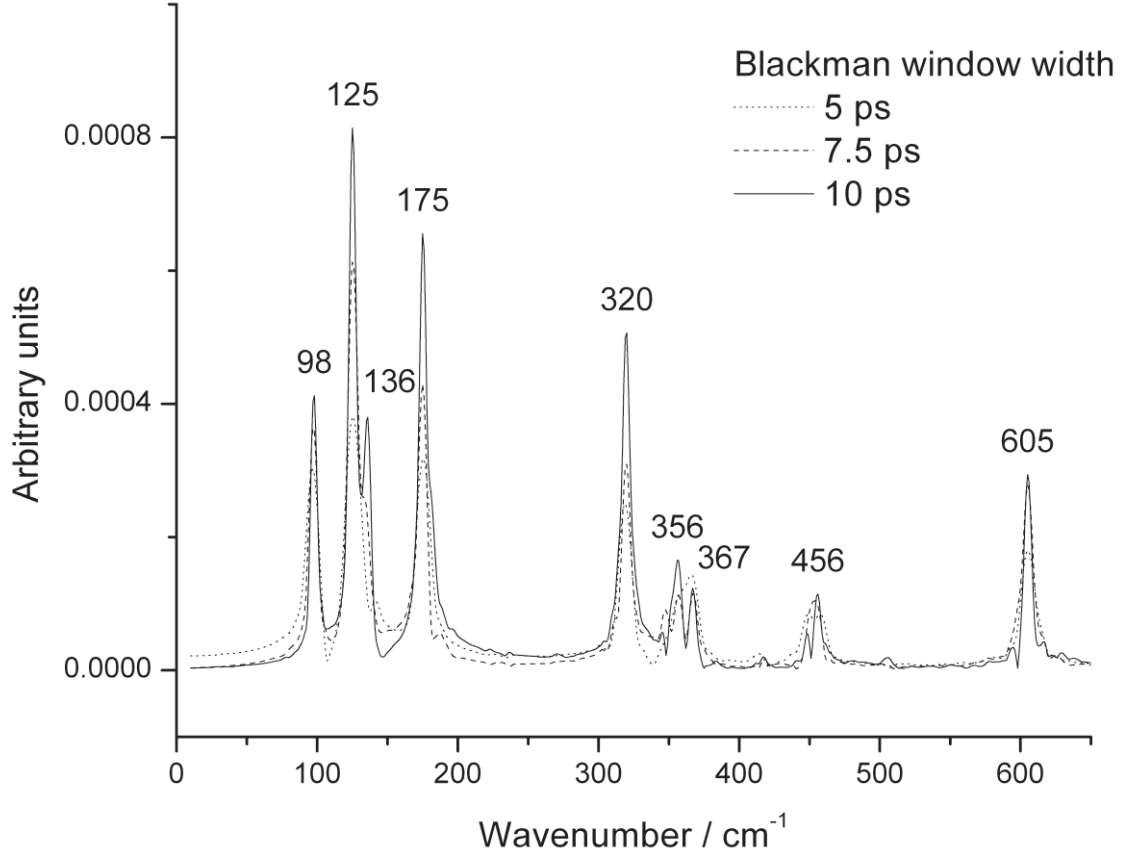
Figure 1 The lattice mode region of the NH_3 phonon spectrum as obtained from the MD trajectory using three Blackman windowing functions of different widths.

The eigenvectors for each mode were extracted and the symmetry assigned by observation of the corresponding atomic motions. In particular, we discriminate between modes that preserve the three-fold axis of the system (*A* symmetry) or the two-fold axes (*E* symmetry). The remaining modes are then assigned as having *F* symmetry. We validate these assignments by comparison with the results of the harmonic lattice-dynamics calculations. The resultant MD peak positions and assignments are tabulated together with the comparable experimental data in Table 4.

Lattice Dynamics Calculations. The lattice-dynamics results obtained with a variety of Hamiltonians and basis sets are also presented in Table 4. The optimized structures appropriate to each method were used, as presented in Table 2. The frequencies of the acoustic modes are imaginary (i.e. negative) but are reasonably close to zero in each case, and neither tighter convergence tolerances nor normalization of the dynamical matrix improves upon these values. The best agreement between the MD normal modes and lattice dynamics frequencies is obtained with the B3LYP/TZP combination, whereas the PW91/TZP frequencies are apparently shifted to a higher frequency by 15–30 cm^{-1}.

Table 4 The character, C (T = translational, L = librational), irreducible representation, I, IR and Raman activities ($\checkmark$ = active, $\times$ = inactive) and frequencies (cm^{-1}) of the external motions obtained from lattice-dynamics calculations and the MD velocity autocorrelation function, along with experimental frequencies and assignments.

| Mode | C | I | IR | Raman | Lattice dynamics calculated frequencies | | | | MD VAF[a] | | Experimental | |
					B3LYP TZP	B3LYP 6-311G**	B3PW91 6-311G**	PW91 TZP	Frequency	I	Frequency	I
1	T	F	$\checkmark$	$\checkmark$	-9.4	-9.0	-8.8	-7.9	—	—	—	—
2	T	E	$\times$	$\checkmark$	98.1	99.7	93.8	111.2	98	E	107[b]	A
3	T	A	$\times$	$\checkmark$	121.6	113.4	120.2	142.2	125	A	138[b]	E
4	T	F	$\checkmark$	$\checkmark$	130.9	132.6	127.5	144.9	136	F	138[c]	F
5	T	F	$\checkmark$	$\checkmark$	174.8	177.0	174.5	191.5	175	F	181[c]	F
—	—	—	—	—	—	—	—	—	—	—	260[b]/258[c]	F
—	—	—	—	—	—	—	—	—	—	—	298[b]	A
6	L	F	$\checkmark$	$\checkmark$	322.0	321.8	331.3	365.4	320	F	310[b]	E
7	L	A	$\times$	$\checkmark$	353.5	348.5	357.8	399.8	356	A	358[b]/361[c]	F
8	L	E	$\times$	$\checkmark$	355.2	354.4	360.8	387.7	367	E	—	—
9	L	F	$\checkmark$	$\checkmark$	449.8	455.3	464.2	485.6	457	F	426[b]	F
10	L	F	$\checkmark$	$\checkmark$	616.4	619.4	625.6	651.4	605	F	532[c]	F

[a] This work. [b] Ref. 3. [c] Ref. 5.

The LO-TO split frequencies obtained from B3LYP/6-311G** calculations with an ε^∞ value of 1.9 are presented in Table 5, along with the IR intensities calculated from the dynamical charge tensors, the scalar magnitudes of which are $Z*(N) = -0.817\ e$ and $Z*(H) = +0.272\ e$. We see immediately that some of the calculated intensities are very low, which may explain the experimental difficulties encountered in trying to resolve and assign these peaks. Further, it should be noted that the IR probe beam is not expected to couple to the LO modes, whereas both polarizations are in principle observable by Raman spectroscopy. The results indicate that it is only the last two external modes that show any significant LO-TO splitting, amounting to 56 and 10 cm^{-1} respectively. The splittings obtained for other values of ε^∞ are presented in Table 6; though there is some variation, we note that the overall distribution of the modes does not change, supporting the use of the liquid-phase value.

Table 5 The character, C (T = translational, L = librational), irreducible representation, I, IR and Raman activities (✓ = active, × = inactive), frequencies, ω (cm^{-1}) and IR absorption intensities, Int (km mol^{-1}) of the external modes in the ammonia phase I B3LYP/6–311G** calculation. Frequencies and intensities of the LO and TO components are presented separately, where appropriate.

Mode	C	I	IR	Ram	ω(LO)	ω(TO)	Int(LO)	Int(TO)
1	T	*F*	✓	✓	-9.0		0.4	
2	T	*E*	×	✓	99.7		0.0	
3	T	*A*	×	✓	113.4		0.0	
4	T	*F*	✓	✓	134.3	132.6	(5.1)	10.4
5	T	*F*	✓	✓	177.7	177.0	(3.3)	6.2
6	L	*F*	✓	✓	321.9	321.8	(0.9)	2.4
7	L	*A*	×	✓	348.5		0.0	
8	L	*E*	×	✓	354.4		0.0	
9	L	*F*	✓	✓	511.8	455.3	(765.8)	997.9
10	L	*F*	✓	✓	628.9	619.4	(255.9)	142.1

Table 6 The external mode LO-TO splittings (cm^{-1}) obtained for different values of the optical dielectric constant, ε^{∞}.

Mode	LO-TO Splitting					
	$\varepsilon^{\infty} = 1.3$	$\varepsilon^{\infty} = 1.5$	$\varepsilon^{\infty} = 1.7$	$\varepsilon^{\infty} = 1.9$	$\varepsilon^{\infty} = 2.1$	$\varepsilon^{\infty} = 2.3$
4	2.15	1.96	1.81	1.68	1.56	1.46
5	1.01	0.92	0.84	0.78	0.73	0.68
6	0.17	0.16	0.15	0.14	0.13	0.12
9	75.56	68.01	61.73	56.46	51.98	48.15
10	16.07	13.12	11.05	9.53	8.37	7.46

Final lattice-mode assignments. A significant number of differences have arisen between the theoretical and experimental assignments of the irreducible representations of the modes. We split the low-frequency spectrum into separate regions, and discuss each in detail.

Modes from 0 to 200 cm^{-1}

The positions of the MD phonon modes in this region coincide reasonably well with those of the experimentally observed bands. However, the theoretical symmetry assignments differ notably from the experimental ones. The first three modes in this region are assigned as *E*, *A* and *F*, respectively, by both the MD and lattice dynamics simulations. However, the previous experimental assignments have included *A* (107 cm^{-1}), *E* (138 cm^{-1}) and *F* (138 cm^{-1}) by Binbrek and Anderson,[3] *A* (98.6 cm^{-1}), *E* (98.6 cm^{-1}) and *F* (131 cm^{-1}) from C-INS[5] and finally *E* (122 cm^{-1}), *F* (130 cm^{-1}) and *A* (143 cm^{-1}) from the atom-atom model calculations.[4] The final mode in this region is found at 175 cm^{-1} in the MD spectrum and, in line with the lattice dynamics and all previous experimental and theoretical work, is assigned *F* symmetry. We note again that the frequencies obtained from the B3LYP/TZP and B3LYP/6-311G** lattice dynamics calculations are slightly shifted to high frequency with respect to the MD results, but are in reasonable agreement overall. The PW91/TZP lattice-dynamics frequencies are shifted by 15–30 cm^{-1} in comparison with the B3LYP/6-311G** and MD results.

Mode at 260 cm^{-1}

Several experiments have suggested the presence of a fundamental mode at 260 cm^{-1}, but the assignments have generally been made on the basis of very weak peaks[3] or have been derived indirectly from observations in deuteroammonia[5] or from combination bands.[6] The observation[7] of a peak at around 280 cm^{-1} at a temperature of 187.6 K may originate from the modes found at around 300 cm^{-1} in other experiments. It is clear that no mode in the region of 260 cm^{-1} is obtained from either the MD or lattice dynamics calculations, in agreement with the results of our previous rigid molecule MD simulations.[2] We note further that combining the results from each of the experimental studies, as in Table 4, yields more than the total of nine low frequency modes that would be anticipated for the ideal material. We suggest therefore that the modes in the vicinity of 260 cm^{-1} may originate from regions of the crystal in which the local coordination of molecules differs from that of the perfect phase I lattice, due perhaps to the presence of lattice defects, or to domains of the metastable and amorphous forms that have manifested themselves previously.[21]

Modes from 290 to 320 cm^{-1}

The current study obtains a single mode in this region at approximately 320 cm^{-1}. The experimental studies suggest modes at 298 and 310 cm^{-1},[3] as did the previous rigid-molecule MD simulations.[2] An analysis of the MD eigenvectors suggests that this mode possesses *F* symmetry, in contrast with the *E* (310 cm^{-1}) assignment for the nearby experimental mode. The lattice dynamics calculations also provide only one band in this region (at 322 cm^{-1} in the B3LYP/6-311G** and B3LYP/TZP methods, and at 331 cm^{-1} in B3PW91/6-311G**), and all the calculations concur upon the assignment of *F* symmetry to this mode. We note, though, that the previous rigid molecule MD simulation used a 2×2×2 supercell of ammonia, and that this could conceivably lead to the incorporation of some fraction of the LO-TO splitting if it were present. Furthermore, the two experimental peaks at 298 and 310 cm^{-1} were obtained from a Raman measurement, which would be expected to detect both optical polarizations. However,

15

the current lattice dynamics calculations suggest that there is only a very small (~0.1 cm^{-1}) splitting of this mode.

Modes from 350 to 500 cm^{-1}

Three modes are observed in the MD spectrum in this region, with symmetry assignments of *A* (356 cm^{-1}), *E* (367 cm^{-1}) and *F* (457 cm^{-1}) respectively. The lattice dynamics calculations also predict three modes in this region, at 348, 354 and 455 cm^{-1} (B3LYP/6-311G**) with *A*, *E* and *F* symmetries respectively, except in the PW91/TZP method, which yields the order *E* (387 cm^{-1}), *A* (399 cm^{-1}) and *F* (487 cm^{-1}). The experimental observations in this region vary. Binbrek and Anderson found one LO-TO split *F* mode in this region at 358 cm^{-1} (TO) and 426 cm^{-1} (LO).[3] The current MD simulation used a single unit cell, which does not include any of the long-range electrostatic interactions. Turning to the lattice dynamics calculations, we find only one mode in the range 400–500 cm^{-1}, namely a TO peak at 455 cm^{-1}. The Raman measurements produced a wide band in the range 325–375 cm^{-1},[6] which may correspond to the two peaks obtained at 356 and 367 cm^{-1} in the present work. Given the absence of LO-TO splitting in the MD simulations, we conclude that it is very likely that the experimental peaks reported by Binbrek and Anderson at 358 and 426 cm^{-1} are two separate modes and not a single LO-TO split *F* mode as previously assigned.

Lattice mode above 500 cm^{-1}

The final lattice mode is observed in experiments at 532 cm^{-1}.[3] The MD simulation shows a peak at 605 cm^{-1}, while the lattice dynamics results are higher still at 625 cm^{-1} (B3LYP/6-311G**) or 651 cm^{-1} (PW91/TZP). All theoretical methods agree with the experimental assignment of *F* symmetry. The LO-TO splitting calculations in the B3LYP/6-311G** method do suggest that there is an LO branch of the 455 cm^{-1} mode at 512 cm^{-1}. The peak is quite close to the experimental value for the final mode and it is possible that it may have been incorrectly assigned. The only experimental evidence for a higher

frequency lattice mode emerges from the C-INS study, in which an F band (574 cm^{-1}) is inferred from the scaling of a deuteroammonia peak.[5]

It should be noted that the comparable experimental studies have been performed at a range of temperatures, which will inevitably lead to some variations in peak positions as compared with our MD simulations obtained at 77 K. Given these limitations, we find that some of our peak positions agree extremely well with the experiment data, and we note that the calculations obtain the correct number of modes for each symmetry type (i.e. $2A + 2E + 5F$).

3.3. Phase I ND$_3$ Lattice Modes. The nine lattice modes in ND$_3$ have also been determined from MD and lattice dynamics calculations. The time-averaged structure determined from the MD trajectory is presented in Table 7.

Table 7 The fractional coordinates of the asymmetric unit in ND$_3$ averaged over the 30 ps PW-DFT MD trajectory.

D$_x$	0.3520
D$_y$	0.2697
D$_z$	0.0965
N$_x$	0.1974

Table 8 compares the NH$_3$ and ND$_3$ lattice modes obtained from the MD and lattice dynamics calculations and tabulates the ratios of their frequencies. The LO-TO splittings obtained from B3LYP/6-311G** calculations are presented in Table 9. We can see that the trend in the values is similar to that observed in the protonated material, although the sizes of the splittings are generally reduced, particularly for the librational modes. The general reduction in the IR intensities is in keeping with the smaller amplitudes of motion expected for vibrations in the deuterated material.

Table 8 NH$_3$ and ND$_3$ lattice mode frequencies (cm^{-1}) and ratios of frequencies as determined from the MD velocity autocorrelation function and lattice dynamics calculations at the B3LYP/TZP level of theory.

NH$_3$ lattice mode		ND$_3$ lattice mode		Ratio of frequencies	
MD	Lattice Dynamics	MD	Lattice Dynamics	MD	Lattice Dynamics
98	98	88	89	1.11	1.10
125	121	114	110	1.09	1.10
136	130	122	120	1.11	1.09
175	174	164	163	1.07	1.08
320	322	225	228	1.42	1.41
356	353	260	257	1.36	1.37
367	355	266	260	1.38	1.37
457	449	326	323	1.40	1.39
605	616	445	448	1.36	1.38

Table 9 The character, C (T = translational, L = librational), irreducible representation, I, IR and Raman activities (✓ = active, × = inactive), frequencies, ω(cm^{-1}) and IR absorption intensities, Int (km mol^{-1}) of the external modes in the ND$_3$ B3LYP/6–311G** calculation. Frequencies and intensities of the LO and TO components are presented separately, where appropriate.

Mode	C	I	IR	Ram	ω(LO)	ω(TO)	Int(LO)	Int(TO)
1	T	*F*	✓	✓	-8.2		0.31	
2	T	*E*	×	✓	90.5		0.0	
3	T	*A*	×	✓	103.1		0.0	
4	T	*F*	✓	✓	123.2	121.6	(4.5)	9.3
5	T	*F*	✓	✓	165.4	164.6	(3.1)	6.2
6	L	*F*	✓	✓	228.3	228.1	(0.7)	1.7
7	L	*A*	×	✓	253.4		0.0	
8	L	*E*	×	✓	259.3		0.0	
9	L	*F*	✓	✓	365.6	326.3	(385.0)	494.2
10	L	*F*	✓	✓	457.3	450.6	(126.9)	76.0

The effects of deuteration on the translational mode frequencies can be rationalized within a simple intermolecular bond-stretching model, assuming that the molecules undergo rigid displacements. The total masses of the protonated and deuterated molecules at 17.024 and 20.045 amu, respectively, leading to reduced masses for stretching motions, μ^p and μ^d, of 8.512 and 10.022 amu, respectively, and a ratio of protonated (ω^p) and deuterated (ω^d) harmonic frequencies given by

$$\frac{\omega^p}{\omega^d} = \sqrt{\frac{\mu^d}{\mu^p}} = 1.085 \,, \qquad (1)$$

in good agreement with the ranges of 1.08–1.10 and 1.07–1.11 obtained from B3LYP/TZP lattice dynamics and MD calculations respectively. Similarly, the effects of deuteration upon the librational-mode frequencies can be modelled within an approximation in which these modes are assumed to involve small torsional oscillations of rigid molecules. In this case the harmonic frequencies vary as $I^{-\frac{1}{2}}$, where the moment of inertia, $I = \sum m_i r_i^2$, clearly scales linearly with the mass of the rotating particles. Thus the frequency ratio depends directly upon the proton and deuteron masses, m^p and m^d respectively, and varies as

$$\frac{\omega^p}{\omega^d} = \sqrt{\frac{m^d}{m^p}} = 1.414 \,, \qquad (2)$$

which is also in good agreement with the ranges 1.37–1.41 and 1.36–1.42 obtained from the B3LYP/TZP lattice dynamics and MD calculations, respectively. We conclude that the first four modes possess translational character, while the remaining five modes are librational. The small range in the frequency ratios is likely due to deviations from purely rigid molecule motion.

3.4 NH$_3$ and ND$_3$ Internal Modes. The lattice dynamics calculations also allow us to define

unambiguously a set of symmetry coordinates with which to describe the internal motions of the system.

These modes can be envisaged as being composed of various in-phase and out-of-phase combinations of

the *A* and *E* symmetry vibrations that are obtained for the isolated molecule. The symmetry coordinates

are presented in Table 10 together with the lattice dynamics frequencies determined at the B3LYP/TZP

level. The normal modes are described in terms of the nine symmetry coordinates (R_{1-3}, β_{1-3} and α_{1-3}) of

the NH$_3$ molecule, as defined in Figure 2. The four molecules in the phase I unit cell are labeled A-D

and occupy the positions shown in Figure 3. The corresponding internal mode region of the NH$_3$ MD

phonon spectrum is show in Figure 4. We note in particular the Davydov (or factor group) splittings of

the modes; these are the small differences in frequency that separate vibrations in which the individual

molecules undergo essentially identical internal motions.

Table 10 Frequencies (cm^{-1}), symmetry coordinates, type of motion and irreducible representation, I, for the Γ-point internal vibrations in NH$_3$ as determined from lattice dynamics calculations. See Figs. 3 and 4 for descriptions of the coordinates used.

	Frequency	Symmetry Coordinates	Motion	I
1	3539	$A(R_2 + R_3 - R_1) + B(R_3 + R_1 - R_2) + C(R_3 - (R_1 + R_2)) + D(R_1 - (R_2 + R_3))$	Asym. Stretch	F
2	3539	$A(R_3 - (R_1 + R_2)) + B(R_1 + R_2 - R_3) + C(R_1 - (R_2 + R_3)) + D(R_1 + R_3 - R_2)$	Asym. Stretch	F
3	3539	$A(R_1 + R_3 - R_2) + B(R_1 - (R_2 + R_3)) + C(R_2 - (R_1 + R_3)) + D(R_1 + R_2 - R_3)$	Asym. Stretch	F
4	3524	$A(R_1 - (R_2 + R_3)) + B(R_2 - (R_1 + R_3)) + C(R_3 - (R_1 + R_2)) + D(R_1 - (R_2 + R_3))$	Asym. Stretch	E
5	3524	$A(R_2 - (R_1 + R_3)) + B(R_1 - (R_2 + R_3)) + C(R_2 - (R_1 + R_3)) + D(R_3 - (R_1 + R_2))$	Asym. Stretch	E
6	3522	$A(R_1 - R_3) + B(R_3 - R_2) + C(R_1 - R_3) + D(R_1 - R_2)$	Asym. Stretch	F
7	3522	$A(R_1 - R_2) + B(R_1 - R_2) + C(R_3 - R_2) + D(R_3 - R_1)$	Asym. Stretch	F
8	3522	$A(R_3 - R_2) + B(R_3 - R_1) + C(R_2 - R_1) + D(R_3 - R_2)$	Asym. Stretch	F
9	3416	$[A - B - C + D](R_1 + R_2 + R_3)$	Sym. Stretch	F

| 10	3416	$[A - B + C - D](R_1 + R_2 + R_3)$	Sym. Stretch	F
11	3416	$[A + B - C - D](R_1 + R_2 + R_3)$	Sym. Stretch	F
12	3403	$[A + B + C + D](R_1 + R_2 + R_3)$	Sym. Stretch	A
13	1732	$A(\beta_3 - (\beta_1 + \beta_2) + \alpha_2 - (\alpha_1 + \alpha_3)) + B(\beta_2 - (\beta_1 + \beta_3) + \alpha_1 - (\alpha_2 + \alpha_3)) + C(\beta_1 + \beta_2 - \beta_3 + \alpha_1 + \alpha_3 - \alpha_2) + D(\beta_3 + \beta_2 - \beta_1 + \alpha_1 + \alpha_2 - \alpha_3)$	Asym. Bend	F
14	1732	$A(\beta_1 + \beta_3 - \beta_2 + \alpha_3 + \alpha_2 - \alpha_1) + B(\beta_3 - (\beta_1 + \beta_2) + \alpha_2 - (\alpha_1 + \alpha_3)) + C(\beta_2 + \beta_3 - \beta_1 + \alpha_1 + \alpha_2 - \alpha_3) + D(\beta_3 - (\beta_1 + \beta_2) + \alpha_1 - (\alpha_2 + \alpha_3))$	Asym. Bend	F
15	1732	$A(\beta_1 - (\beta_2 + \beta_3) + \alpha_3 - (\alpha_2 - \alpha_1)) + B(\beta_2 + \beta_3 - \beta_1 + \alpha_1 + \alpha_2 - \alpha_3) + C(\beta_1 + \beta_3 - \beta_2 + \alpha_2 + \alpha_3 - \alpha_1) + D(\beta_1 + \beta_2 - \beta_3 + \alpha_2 - (\alpha_1 + \alpha_3))$	Asym. Bend	F
16	1699	$A(\beta_1 - \beta_3 + \alpha_3 - \alpha_2) + B(\beta_2 - \beta_1 + \alpha_1 - \alpha_3) + C(\beta_2 - \beta_1 + \alpha_1 - \alpha_2) + D(\beta_1 - \beta_3 + \alpha_3 - \alpha_2)$	Asym. Bend	F
17	1699	$A(\beta_1 - \beta_2 + \alpha_3 - \alpha_1) + B(\beta_1 - \beta_3 + \alpha_3 - \alpha_2) + C(\beta_1 - \beta_2 + \alpha_3 - \alpha_1) + D(\beta_2 - \beta_3 + \alpha_1 - \alpha_3)$	Asym. Bend	F
18	1699	$A(\beta_2 - \beta_3 + \alpha_1 - \alpha_2) + B(\beta_2 - \beta_3 + \alpha_1 - \alpha_2) + C(\beta_3 - \beta_2 + \alpha_2 - \alpha_3) + D(\beta_2 - \beta_1 + \alpha_1 - \alpha_3)$	Asym. Bend	F
19	1679	$A(\beta_2 + \beta_3 - \beta_1 + \alpha_2 - \alpha_3) + B(\beta_2 + \beta_3 - \beta_1 + \alpha_1 - \alpha_3) + C(\beta_1 + \beta_3 - \beta_2 + \alpha_2 - \alpha_1) + D(\beta_1 + \beta_2 - \beta_3 + \alpha_3 - \alpha_2)$	Asym. Bend	E
20	1679	$A(\beta_2 - (\beta_1 + \beta_3) + \alpha_1 - (\alpha_2 + \alpha_3)) + B(\beta_3 - (\beta_1 + \beta_2) + \alpha_2 - (\alpha_1 + \alpha_3)) + C(\beta_1 - (\beta_2 + \beta_3) + \alpha_3 - (\alpha_1 + \alpha_2)) + D(\beta_2 - (\beta_1 + \beta_3) + \alpha_2 - (\alpha_2 + \alpha_3))$	Asym. Bend	E
21	1210	$[A + B + C + D](\alpha_1 + \alpha_2 + \alpha_3)$	Inversion	A
22	1170	$[A - B - C + D](\alpha_1 + \alpha_2 + \alpha_3)$	Inversion	F
23	1170	$[A - B + C - D](\alpha_1 + \alpha_2 + \alpha_3)$	Inversion	F
24	1170	$[A + B - C - D](\alpha_1 + \alpha_2 + \alpha_3)$	Inversion	F
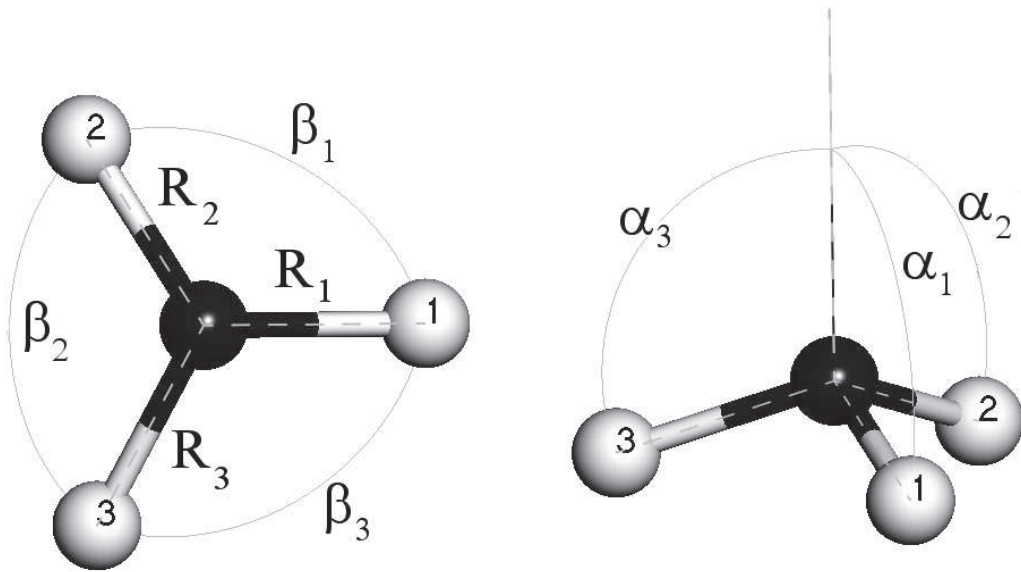
Figure 2 The symmetry coordinates of a single NH_3 molecule. Black and white spheres represent nitrogen and hydrogen atoms respectively.
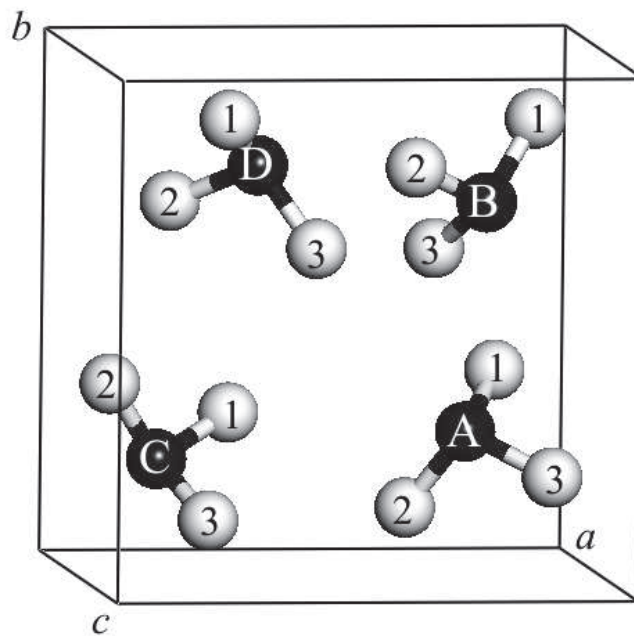
Figure 3 The unit cell of phase I ammonia, showing the labels of hydrogen atoms (1 to 3) and molecules (A to D).
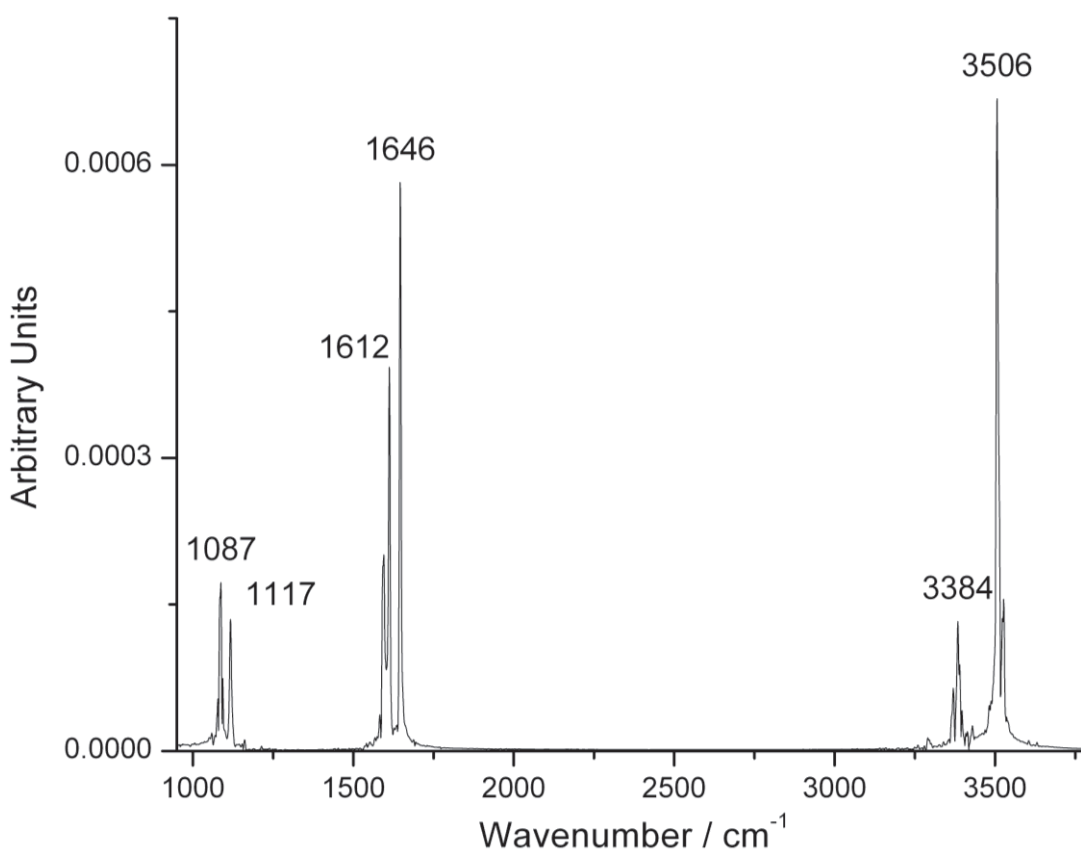
Figure 4 Internal mode region of the NH_3 phonon spectrum as determined from the MD velocity autocorrelation function.

The resolution in this region of the MD phonon spectrum and of the experimental results is too low to enable us to discriminate each separate mode, though we note that some separate peaks are visible in Figure 4. We can easily assign the peaks in the various regions of the MD phonon spectrum, and these data are presented in Table 11 for ND_3 and NH_3, along with the comparable experimental results. The frequencies of the bending and inversion modes are in good agreement with the experimental values, whereas the stretching frequencies are consistently overestimated. It is common practice to scale theoretical bond-stretching frequencies by a factor that depends upon the Hamiltonian used, but which is typically in the range 0.90 – 0.99.[22] We note that a scaling of this magnitude would bring our values into close agreement with experiment. The lattice dynamics stretching frequencies greatly overestimate the experimental values, but this is to be expected given that they are obtained within a harmonic approximation. We can attempt to treat the anharmonicity of these modes by first obtaining the potential

energy curve for a representative N–H stretching motion, and then solving the associated one-dimensional Schrödinger equation by numerical integration.[23,24] The totally symmetric stretch (mode 12 in Table 10) is a particularly convenient choice, for it can be modeled without reduction in lattice symmetry. The potential was determined as a sixth-order polynomial fit to the total energies obtained at seven N–H bond lengths, yielding a fundamental anharmonic absorption that is much closer to experiment at 3304 cm^{-1}, and a first overtone band at 6445 cm^{-1}. A comparison of this result with the frequencies in Table 10 yields an anharmonic correction for the symmetric stretching modes of the order 100 cm^{-1}. It is reasonable to assume that all the harmonic asymmetric stretching frequencies are in error by similar amounts.

Table 11 Assignments and frequencies (cm^{-1}) of the internal modes of NH_3 and ND_3 as determined from MD simulations together with experimental results.

Assignment	NH_3		ND_3	
	MD simulation	Experimental[a]	MD simulation	Experimental[a]
Asymmetric Stretches	3506	3375	2602	2511
Symmetric Stretches	3384	3210	2424	2342
Angle Bends	1612–1646	1650	1191	1195
Inversions	1087–1117	1057	820	813

[a] Ref. 21.

4. Conclusions. The complete zone-center phonon spectrum of ammonia has been obtained from a combined MD and lattice dynamics approach. The symmetry of each peak has been assigned using both methods, resulting in significant changes to the previous experimental and theoretical assignments of the lattice mode region. The frequencies of the internal modes have also been calculated, and are found to be in good agreement with experiment.

The work highlights the benefits of applying a combination of theoretical approaches to the calculation of the vibrational properties of a material. The lattice-mode eigenvalues obtained from the PW-DFT MD simulations are in excellent agreement with experimental frequencies, despite the fact that the trajectories were limited to 30 ps length. The lattice dynamics calculations also provide a reasonably accurate estimate of the eigenvalues, but we observe that the values are shifted to high frequencies with respect to the MD and previous experimental results. In general, though, the two methods provide mode assignments that are in good agreement. The inclusion of the LO-TO splittings obtained from the lattice dynamics approach is shown to be necessary if a full comparison with the experimental spectra is sought, and we note that MD simulations cannot easily access these values. The methods are also shown to complement each other in the high frequency internal mode region of the spectrum. Again, the MD eigenvalues are generally closer to experiment, but the ability of the lattice dynamics calculations to resolve the closely spaced frequencies of the Davydov-split modes is extremely useful, and allows us to make an unambiguous assignment of each internal mode in terms of a set of symmetry coordinates.

Supporting Information Available: XYZ format movie files of the eigenvectors for each of the NH_3 and ND_3 lattice modes. Graphs of temperature and energy for the MD runs.

References

(1) Boese, R.; Niederpruem, N.; Bläser, D.; Maulitz, A. H.; Antipin, M. Y.; Mallinson, P. R. *J. Phys. Chem.* **1997**, *101*, 5794.

(2) Siddick, M. M.; Ackland, G. J.; Morrison, C. A. *J. Chem. Phys.* **2006**, *125*, 64707.

(3) Binbrek, O. S.; Anderson, A. *Chem. Phys. Lett.* **1972**, *15*, 421.

(4) Righini, R.; Neto, N.; Califano, S.; Walmsley, S. H. *Chem. Phys.* **1978**, *33*, 345.

(5) Powell, M.; Dolling, G.; Pawley, G. S.; Leech, J. W. *Can. J. Phys.* **1980**, *58*, 1703.

(6) Reding, F. P.; Hornig, D. F. *J. Chem. Phys.* **1951**, *19*, 594.

(7) Nye, C. L.; Medina F. D. *Phys. Rev. B* **1985**, *32*, 2510.

(8) Allen, M. P.; Tildesley, D. J. *Computer Simulation of Liquids*; Oxford University Press, 1987.

(9) Harris, F. J. *Proc. IEEE* **1978**, *66*, 51.

(10) Cardini, G. G.; Schettino, V. *Chem. Phys.* **1990**, *146*, 147.

(11) Cardini, G. G.; O'Shea, S. F.; Marchese, M.; Klein, M. L. *Phys. Rev. B* **1985**, *32*, 4261.

(12) Anderson, D. C.; Kieffer, J.; Klarsfeld, S. *J. Chem. Phys.* **1993,** *98*, 8978.

(13) Born, M.; Huang K. *Dynamical Theory of Crystal Lattices*; Oxford University Press, 1998.

(14) Baroni, S.; de Girconoli, S.; Dal Corso, A.; Giannozzi, P. *Rev. Mod. Phys.* **2001**, *73*, 515.

(15) Hewat, A. W.; Riekel, C. *Acta Crystallogr., Sect. A: Cryst. Phys., Diffr., Theor. Gen. Cryst.*, **1979**, *35*, 569.

(16) Clark, S. J.; Segall, M. D.; Pickard, C. P.; Hasnip, P. J.; Probert, M. J.; Refson, K.; Payne, M. C. *Z. Kristallogr.* **2005**, *220*, 567.

(17) Dovesi, R.; Saunders, V. R.; Roetti, C.; Orlando, R.; Zicovich-Wilson, C. M.; Pascale, F.; Civalleri, B.; Doll, K.; Harrison, N. M.; Bush, I. L.; D'Arco P.; Llunell, M. *CRYSTAL06 User's Manual*; University of Torino, Torino, 2006.

(18) Pascale, F.; Zicovich-Wilson, C. M.; Lopez, F.; Civalleri, B.; Orlando, R.; Dovesi, R. *J. Comput. Chem.* **2004**, *25*, 888.

(19) Zicovich-Wilson, C. M.; Pascale, F.; Roetti, C.; Saunders, V. R.; Orlando, R.; Dovesi, R. *J. Comput. Chem.* **2004**, *25*, 1873.

(20) Vanderhoff, J. E.; LeMaster, E. W.; McKnight, W. H.; Thompson, J. C. *Phys. Rev. A* **1971**, *4*, 427.

(21) Holt, J. S.; Sadoskas, D.; Pursell, C. J. *J. Chem. Phys.* **2004**, *120*, 7153.

(22) Scott, A. P.; Radom, L. *J. Phys. Chem.* **1996**, *100*, 16502.

(23) Ugliengo, P.; Pascale, F.; Merawa, M.; Labeguerie, P.; Tosoni, S.; Dovesi, R. *J. Phys. Chem. B* **2004**, *108*, 13632.

(24) Pascale, F.; Tosoni, S.; Zicovich-Wilson, C. M.; Ugliengo, P.; Orlando, R.; Dovesi, R. *Chem. Phys. Lett.* **2004**, *396*, 4.